RSC Advances

PAPER

View Article Online
View Journal | View Issue

Cite this: *RSC Adv.*, 2025, **15**, 15366

Preparation and evaluation of the biosynthetic procedure of iron oxide and magnesium oxide nanoparticles using *Hylocereus undatus* fruit peel extract and their anticancer properties†

Sadia Adnin Oyshi,[a] Rumana A. Jahan,[b] Fahima Aktar,[c] Md. Zakir Sultan,[b] Abu Asad Chowdhury,[c] Jakir Ahmed Chowdhury,[d] Shaila Kabir[c] and Md. Shah Amran*[c]

Nanoparticles offer enhanced interactions with other materials owing to their enlarged surface area. This property makes them stronger, more stable and ideal for biomedical applications. Among the various synthetic methods for nanoparticles, biosynthetic method stands out due to its cost-effectiveness and environmentally friendly nature. In this context, we developed novel biosynthetic procedures for iron oxide and magnesium oxide nanoparticles using the extract of *Hylocereus undatus* (dragon fruit) peel, which acted as a reducing agent and capping agent. The biosynthesized nanoparticles were characterized using different techniques, such as ultraviolet-visible (UV-VIS) spectrophotometry, transmission electron microscopy (TEM), energy dispersive X-ray spectroscopy (EDX), Fourier-transform infrared spectroscopy (FTIR) and X-ray diffractometry (XRD). To evaluate their anticancer properties, the nanoparticles were tested on HeLa cells (derived from human cervical carcinoma) and BHK-21 cells (obtained from baby hamster kidney fibroblasts) and compared with the negative control group (dimethyl sulfoxide) and standard group (*Hylocereus undatus* fruit peel extract). Results showed that only less than 5% HeLa cells survived in both cases, and less than 5% and 60% BHK-21 cells survived on administering magnesium oxide and iron oxide nanoparticles, respectively, which were quite better than the results obtained for the standard and negative control groups. This study reports a safe and rapid method for the biosynthesis of iron oxide and magnesium oxide nanoparticles using *Hylocereus undatus* fruit peel extract and demonstrates their potential as anticancer agents. These findings suggest that iron oxide and magnesium oxide nanoparticles warrant further investigation for the development of more effective and safe anticancer drug formulations.

Received 16th October 2024
Accepted 3rd March 2025

DOI: 10.1039/d4ra07411d

rsc.li/rsc-advances

Introduction

Nanotechnology is a crucial field of the modern world that deals with nanometer scale materials, which falls typically in the 1–100 nanometer range.[1] It is applied for industrial, medicinal and energy purposes, exhibiting potential results in each of these sectors. Moreover, nanoparticles are noted for their small size, high surface area-to-volume ratio, and unique optical, magnetic, chemical, and mechanical properties.[2] These characteristics make them promising candidates for biomedical applications, especially as antioxidant and anticancer agents.[3] Although various chemical and physical methods are used to synthesize nanoparticles, they often involve hazardous and toxic chemicals. In contrast, biosynthesis strategies of metal nanoparticles are better than other strategies due to the low toxicity, cost-effectiveness, eco-friendliness, reduced time requirements and higher control ability in composition and distribution of the particle structure offered by these methods. Generally, the biosynthesis procedure includes a biological compound as a capping and reducing agent and a precursor.[4,5] In our study, we used *Hylocereus undatus* fruit peel (HUFP) as the biological compound and iron chloride hexahydrate ($FeCl_3 \cdot 6H_2O$) and magnesium nitrate hexahydrate ($Mg(NO_3)_2 \cdot 6H_2O$) as precursors to form iron oxide (Fe_2O_3NPs) and magnesium oxide nanoparticles (MgONPs). The reason behind choosing HUFP as the biological compound was because it contains chemical compounds, such as betanin, phyllocactin, hylocerenin, betacyanin, pectin,

[a]*Department of Pharmacy, East West University, Dhaka, Bangladesh. E-mail: Sadia02021@gmail.com*

[b]*Centre for Advanced Research in Sciences (CARS), University of Dhaka, Bangladesh*

[c]*Department of Pharmaceutical Chemistry, University of Dhaka, Bangladesh. E-mail: fahima@du.ac.bd; amranms@du.ac.bd*

[d]*Department of Pharmaceutical Technology, University of Dhaka, Bangladesh*

† Electronic supplementary information (ESI) available. See DOI: https://doi.org/10.1039/d4ra07411d

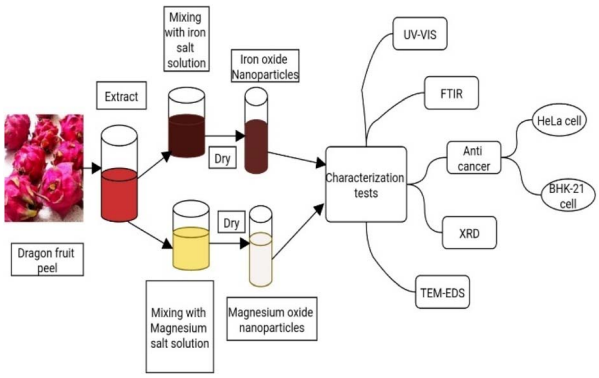

Fig. 1 Schematic of the biosynthesis of the nanoparticles and their characterization tests.

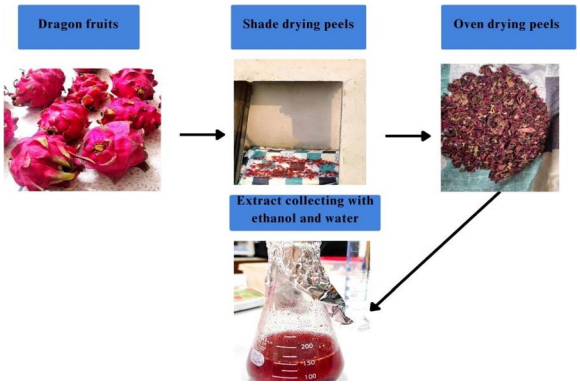

Fig. 2 Collection process of peel extract.

triterpenoids, and steroids,[6,7] which exhibit various pharmacological effects against tumors, inflammation and oxidation.[8,9] The antioxidant activity was particularly notable because these compounds could donate electrons to neutralize free radicals, indirectly suggesting that the organic compounds in dragon fruit peel might be capable of reducing metal salt ions in the synthesis of metal nanoparticles.

Fe_2O_3NPs possess ferro-, ferri-, or super-magnetic properties that enhance their ability to reach specific organs using an external magnetic field. Their high reactivity can be localized within tumor cells through various methods and drive their potential use.[10] When these NPs release ferrous or ferric ions in the acidic environment of lysosomes during endocytosis, it triggers Fenton and Haber–Weiss reactions, producing reactive oxygen species (ROS). This process leads to lipid peroxidation and damage to intracellular macromolecules in cancer cells.[11,12] On the other hand, magnesium oxide (MgO) NPs exhibit anticancer properties through several key mechanisms. They induce ROS production, leading to the damage and death of cancer cells, which are particularly susceptible to oxidative stress. MgONPs trigger apoptosis in cancer cells, reducing their number. They show selective toxicity towards cancer cells over normal cells due to differences in cellular environments.[13,14] Additionally, MgONPs disrupt mitochondrial function, causing loss of membrane potential and cell death, and can arrest the cancer cell cycle, preventing proliferation. These mechanisms make MgONPs promising for cancer therapy, with ongoing research aimed at optimizing their clinical use.[15] Using HUFP extract here as biological agent we are trying to biosynthetically create iron oxide and magnesium oxide nanoparticles and study their anticancer effect (Fig. 1).

Experimental

Materials and chemicals

Dragon fruit peel, ferric chloride hexahydrate ($FeCl_3 \cdot 6H_2O$), magnesium nitrate hexahydrate ($Mg(NO_3)_2 \cdot 6H_2O$), deionized water, sodium hydroxide (NaOH), dimethyl sulfoxide (DMSO), HeLa cell line and BHK21 Cell line from Centre for Advanced Research in Sciences (CARS), DMEM (Dulbecco's Modified Eagles' Medium).

Preparation of the extract

Collection of extract from the peel. Fresh *H. undatus* fruits were bought from a local market in Dhaka, Bangladesh. Then, their peels were removed and washed with water. Following that, they were cut into pieces and shade dried for 3 days to expel out the moisture from it and oven dried at 45 °C and turned into fine powder.

For collecting their extract 5 g of the prepared powder was mixed into a 2 : 1 ethanol and deionized water solution in two different 250 mL beakers. Then, the mixture was heated at 34 °C for 1 h. After cooling to room temperature, the solution was filtered through filter paper. Finally, the extract was stored at −4 °C for further use[16] (Fig. 2).

Synthesis of NPs

Synthesis of Fe_2O_3NPs. For the synthesis of Fe_2O_3NPs, HUFP extract was used as the capping agent and ferric chloride hexahydrate ($FeCl_3 \cdot 6H_2O$) was the precursor. Synthesis was done by mixing 1 part of extract with 1 part of iron salt and 1 part of extract with 3 parts of iron salt. For each ratio, 100 mL of extract was added dropwise to 0.1 M $FeCl_3 \cdot 6H_2O$ solution at room temperature. A brownish-black coloured solution confirmed the formation of iron oxide NPs. The pH was adjusted to 11 by adding 1 M NaOH. The mixture was stirred using a magnetic stirrer for 30 min. The prepared nanoparticles were separated *via* centrifugation at 3000 rpm for 20 min and subsequently the nanoparticles were washed with ethanol and water, respectively for 15 minutes. Finally, the obtained NPs were dried in a hot air oven at 70 °C for 3–4 h and stored in an air tight container[17] (Fig. 3a).

Synthesis of MgONPs. The synthesis of MgONPs was done in 1 : 5 ratio of extract and magnesium salt. Magnesium nitrate hexahydrate ($Mg(NO_3)_2 \cdot 6H_2O$) worked as a precursor and HUFP extract worked as a capping agent. Three hundred mL of 1 M of $Mg(NO_3)_2 \cdot 6H_2O$ was taken in a 500 mL beaker and 60 mL of HUFP extract was added dropwise into it while magnetic stirring at 80 °C. To adjust the pH at 12, 1 M of NaOH was added and the resultant mixture was kept stirring for 4 h. As a result, the solution developed a yellowish colloidal appearance which indicated the formation of MgONPs.

To separate the nanoparticles, the solution was centrifuged at 3000 rpm for 10 min. The collected nanoparticles were dried

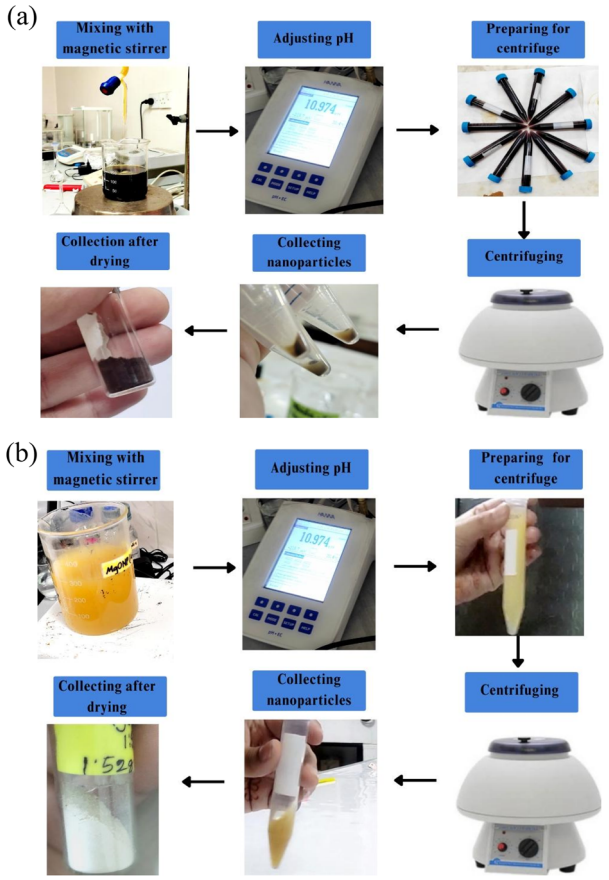

Fig. 3 (a) Biosynthesis procedure of Fe_2O_3NPs. (b) Biosynthesis procedure of MgONPs.

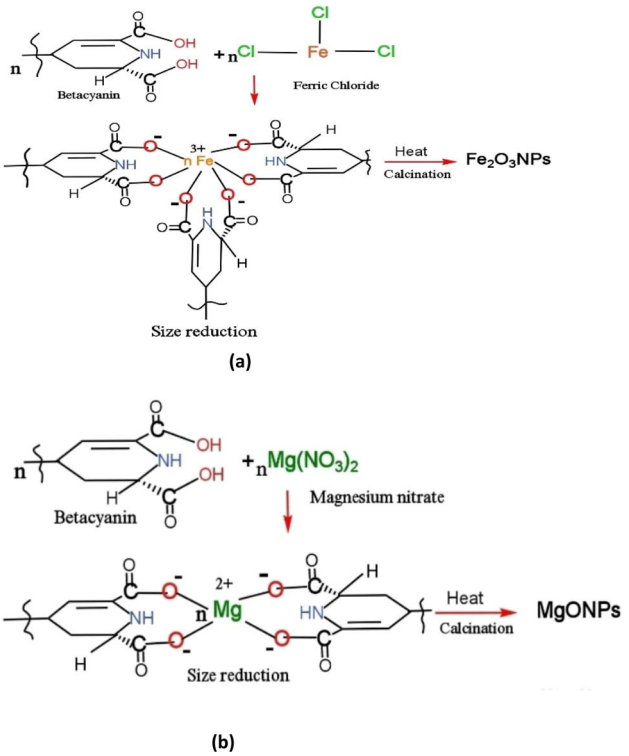

Fig. 4 Plausible chemical reaction mechanisms for forming nanoparticles: (a) Fe_2O_3NPs (b) MgONPs.

in a hot air oven at 50 °C. Later, the final product was calcined in a muffle furnace at 400 °C for 2 h to obtain the white powder of MgONPs[18] (Fig. 3b).

Plausible chemical reaction

HUFP contains numerous phytochemicals, with betacyanin being the most abundant, contributing to its distinct reddish color.[19] The precise mechanisms of the phytosynthesis of biogenic NPs are not fully understood, though several plausible pathways have been proposed. In biosynthesis, phytochemicals found in plant parts often play a crucial role in reducing particle size. Given the wide variety of phytochemicals, it is challenging to pinpoint the specific bio-reductant and stabilizing agents responsible for the production and stabilization of metallic nanoparticles (MNPs). Since betacyanin is the predominant phytochemical in HUFP, we hypothesize that it may act as a reducing agent, aiding in particle size reduction and facilitating the formation of nanoparticles. Notably, betacyanin contains a betalamic acid structure, which may contribute to size reduction by donating electrons through its functional –OH group[20] and possibly through its nitrogen-containing groups as well. The exact stoichiometry and resulting products are likely to vary depending on conditions such as pH, temperature, and pressure. A plausible reaction involving the –OH functional group is illustrated in Fig. 4. The proposed mechanisms for the synthesis of Fe_2O_3 NPs and MgONPs from HUFP extracts are as follows:

(1) An initial interaction occurs between the precursor salt solutions of $FeCl_3$ and $Mg(NO_3)_2$ with the betacyanin-rich HUFP extract, particularly with the betalamic acids present in the extract. (2) As a result of this interaction, Fe–betalamic acid (Fig. 4(a)) and Mg–betalamic acid (Fig. 4(b)) complexes are formed. Here, betalamic acid functions as a reducing agent, with its –OH group contributing to the reduction and control of NP size. (3) Finally, Fe_2O_3 NPs (Fig. 4(a)) and MgONPs (Fig. 4(b)) are synthesized through the heating and calcination of the Fe–betalamic and Mg–betalamic acid complexes at elevated temperatures.

Characterization techniques

The biosynthesized Fe_2O_3NPs and MgONPs were characterized for their wavelength absorption, size, geometry, and structural consequences.

UV-visible spectroscopy

UV-visible spectrophotometry was used to confirm NP formation. The formation of Fe_2O_3NPs and MgONPs was verified by monitoring the surface plasmon resonance band within the 200–800 nm range.

X-ray diffraction (XRD) analysis

XRD was used to examine the crystalline nature of the biosynthesized Fe_2O_3NPs and MgONPs. Powdered samples were

subjected to X-rays in scanning mode, operated at 30 mA current with 40 kV voltage and Cu/Kα radiation with 20–70° in 2θ angles the diffraction pattern was recorded at specific parameters. The resulting diffraction pattern allowed calculation of average crystalline size using the Debye–Scherrer equation:

$$D = k\lambda\beta\cos\theta$$

where, k = shape factor (0.94); λ = X-ray wavelength ($\lambda = 1.5418$ Å); β = full width at half maximum (FWHM) in radians; and θ = Bragg's angle.

Fourier transform infrared (FTIR) spectroscopy

FTIR was employed to identify functional groups involved in Fe_2O_3NP and MgONP synthesis. This technique analyses the sample's infrared absorption spectrum in the 400–4000 cm^{-1} range, providing insight into capping, reduction, and stabilization mechanisms. Prior to analysis, synthesized Fe_2O_3NPs and MgONPs were mixed with KBr to make a transparent pellet.

Transmission electron microscope analysis and energy dispersive X-ray analysis (TEM-EDX)

The size, shape, and morphology of the biosynthesized Fe_2O_3NPs and MgONPs were analysed using a TEM. To prepare the samples for TEM analysis, the Fe_2O_3NPs and MgONPs were dispersed in deionized water using an ultrasonic bath to form a uniform suspension. A drop of this suspension was then applied to a carbon-coated copper grid with a lacey carbon film and left to dry at room temperature. The elemental composition of the synthesized Fe_2O_3NPs and MgONPs was examined through EDX analysis using the same instrument used for capturing TEM images.

Anticancer test

The anti-cancer effect of Fe_2O_3NPs and MgONPs was observed qualitatively and quantitatively. The qualitative test was done by checking cytotoxicity against HeLa and BHK21 cells and the quantitative test was done by checking cytotoxicity against HeLa cells. HeLa and BHK21 cell lines were maintained in DMEM containing 1% penicillin–streptomycin (1 : 1), 0.2% gentamycin, and 10% foetal bovine serum (FBS). HeLa cells (2×10^4/100 μL) and BHK21 cells (1.5×10^4/100 μL) were seeded onto a 96-well plate and incubated at 37 °C in a CO_2 incubator (Nuaire, USA). A 50 μL (30 mg mL^{-1}) sample of Fe_2O_3NPs and 50 μL (3 mg mL^{-1}) of MgONPs (autoclaved) were added to each well for qualitative testing and a 25 μ sample from different doses of Fe_2O_3NPs and MgONPs was applied for quantitative testing. After 48 h of incubation, insoluble samples were washed out with fresh media and cytotoxicity was examined under a trinocular microscope with a camera (Optika, Italy). Duplicate wells were used for each sample.[17,21]

Results and discussion

Analysis of nanoparticles

UV-visible spectroscopy. The UV-visible spectrophotometer was used to analyse the biosynthesis and stability of Fe_2O_3NPs and MgONPs. The absorbance range of 250–400 nm was adjusted to detect the presence and stability of Fe_2O_3NPs and MgONPs. The ideal wavelength of 275 nm was observed in the UV-VIS spectroscopy readings for synthesized Fe_2O_3NPs and MgONPs[22–24] (Fig. 5).

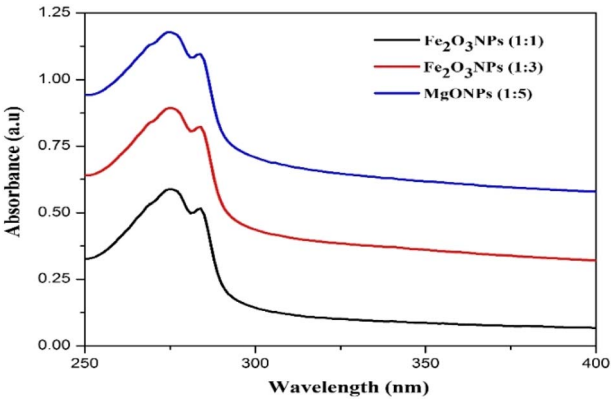

Fig. 5 UV-visible spectrum of Fe_2O_3NPs (1 : 1), Fe_2O_3NPs (1 : 3), and MgONPs (1 : 5).

Fourier transform infrared (FTIR) spectrum. The Fe_2O_3NPs and MgONPs were capped and reduced by secondary metabolites. FTIR spectroscopy was utilized for the detection of secondary metabolites in Fe_2O_3NPs and MgONPs. The FTIR spectra of Fe_2O_3NPs synthesized from HUFP extract exhibited substantial absorption peaks at 474.49 cm^{-1}, 1084.70 cm^{-1}, 1477.47 cm^{-1}, 1627.92 cm^{-1} and 3435.22 cm^{-1} for the 1 : 1 ratio and 478.35 cm^{-1}, 601.79 cm^{-1}, 1083.99 cm^{-1}, 1477.47 cm^{-1}, 1622.13 cm^{-1} and 3427.71 cm^{-1} for the 1 : 3 ratio (Fig. 6). The peaks at 474.49 and 474.35 cm^{-1} ensured the presence of Fe–O bond in the sample.[25,26] The peaks at 3427.71 cm^{-1} and 3435.22 cm^{-1} represent –OH bond stretching from the aqueous phase. Moreover, the peaks at 1477.47 cm^{-1} indicates C–H stretching, 1622.13 cm^{-1} and 1627.92 cm^{-1} indicates C=C stretching, 1084.70 cm^{-1} and 1083.99 cm^{-1} generally indicates

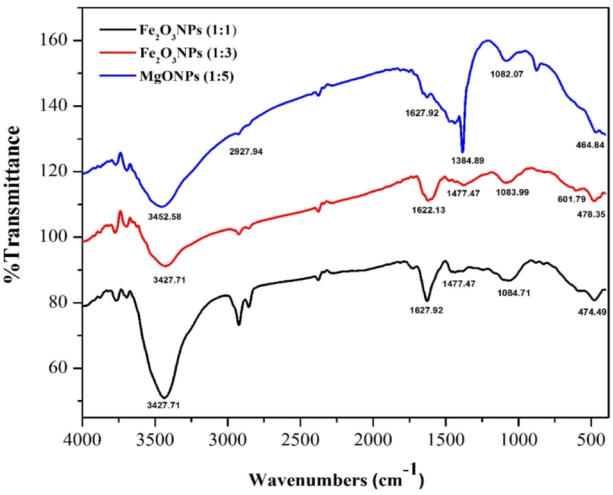

Fig. 6 FTIR spectrum of Fe_2O_3NPs (1 : 1), Fe_2O_3NPs (1 : 3), and MgONPs (1 : 5).

C–O stretching, ensuring the presence of alkane, conjugated alkene and secondary alcohol in the HUFP extract as observed by a previous study.[27]

The peak at 464.84 cm^{-1} ensured the presence of the Mg–O bond in MgONPs (Fig. 6). The peak at 3452.58 cm^{-1} represents –OH bond stretching from the aqueous phase, the peak at 2927.94 cm^{-1} indicates the stretching vibrations of aliphatic C–H bonds, 1627.96 cm^{-1} indicates the presence of C=O stretching of alkenes and the peak at 1384.89 cm^{-1} indicates the bending vibrations of the methyl ($-CH_3$) group. Additionally, the peak at 1082.07 cm^{-1} indicates the presence of functional groups involving C–O stretching vibrations of alcohol.[28]

The shift in peak position in the range of 400–4000 cm^{-1} ensures that these functional groups contain compounds bound to the iron oxide and magnesium oxide surfaces (Fig. 6).

X-ray diffraction (XRD). The crystallinity of the synthesized Fe_2O_3NPs and MgONPs using HUFP extract indicates that the crystal planes of (202) and (431) corresponding to the peaks at 31.716 and 45.455 according to XRD analysis (Fig. 7(a)). The peaks at 31.06, 45.45 and 53.49 correspond to those of (202), (431) and (512) planes, respectively, indicating the formation of Fe_2O_3NPs (1 : 1) and (1 : 3) (Fig. 7(b)). The intense and sharp peaks undoubtedly revealed that Fe_2O_3NPs formed by the reduction method using HUFP extract were crystalline in nature according to Te JCPDS file 019-0629.[29] On the other hand, XRD data of MgONPs (1 : 5) indicates that the crystal planes of (200), (220) and (222) correspond to that of 42, 62.19 and 78.47 which confirms the formation of MgONPs (Fig. 7(c)). They were verified using the JCPDS standard XRD data (no. 01-023-0074).[30,31]

Transmission electron microscopy and energy dispersive X-ray (TEM-EDX). The resultant colloidal particles were characterized to determine the shape and size of nanoparticles using transmission electron microscopy (TEM). Different TEM micrograph images of the synthesized Fe_2O_3NPs and MgONPs were obtained, which are displayed in Fig. 8 and 9. The particle sizes ranged from approximately 6 nm to 14 nm for Fe_2O_3NPs and 14 nm to 20 nm for MgONPs.[32,33]

The EDX spectrum of the materials are depicted in Fig. 10(a) and (b), which show the elemental analysis of the synthesized Fe_2O_3NPs and MgONPs, respectively.[34] This analysis demonstrated a prominent indication of a metallic iron and magnesium area at 6.5 keV and 1.5 keV, respectively and confirmed the formation of Fe_2O_3NPs and MgONPs synthesized through the utilization of HUFP. A high peak of oxygen and moderate signal of copper was observed. Furthermore, low signals for carbon and sodium were detected as a result of the chemicals used in

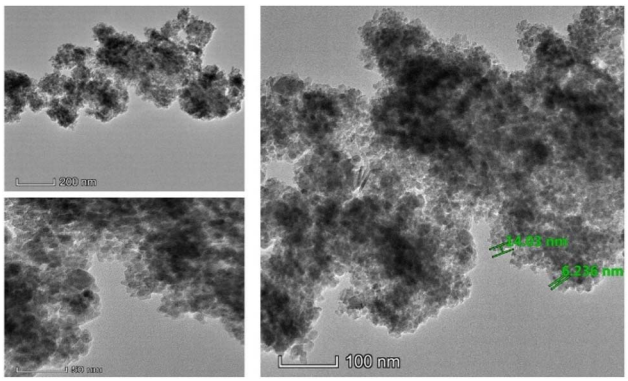

Fig. 8 TEM images of Fe_2O_3 NPs.

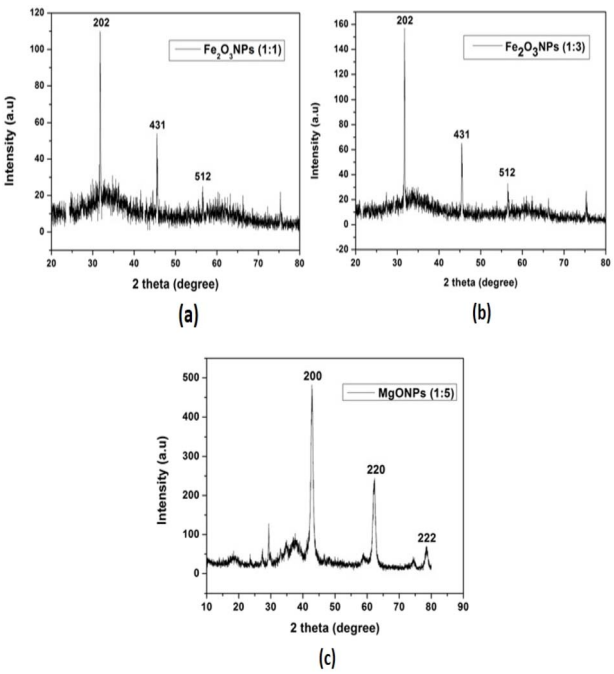

Fig. 7 XRD spectra of nanoparticles: (a) Fe_2O_3NPs (1 : 1), (b) Fe_2O_3NPs (1 : 3) and (c) MgONPs (1 : 5).

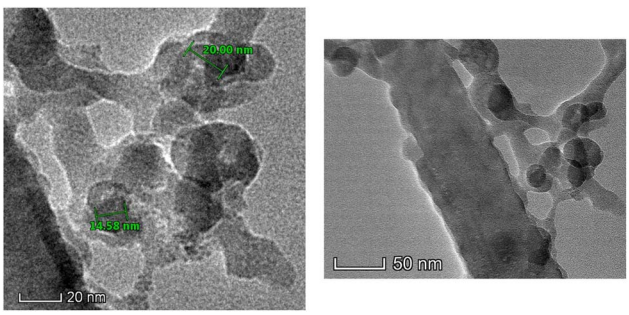

Fig. 9 TEM images of MgONPs.

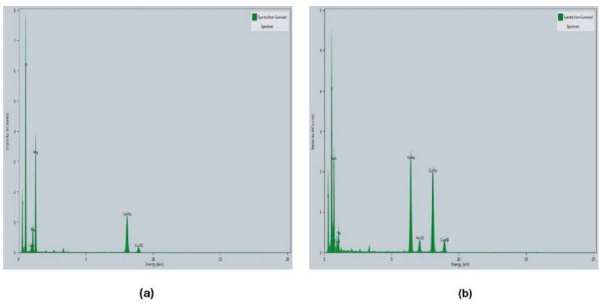

Fig. 10 EDX spectrum of (a) Fe_2O_3 NPs and (b) MgONPs.

Fe_2O_3NP preparation. Similar peaks were observed for MgONPs, which might be due to the use of different chemicals during sample preparation.

Anti-cancer activity. The impact of biosynthesized Fe_2O_3NPs and MgONP on cell viability was investigated qualitatively and quantitatively using two different cell lines: HeLa cells and BHK-21 cells.

Qualitative test. Cytotoxicity was seen in HeLa cells and BHK-21 cells. The cytotoxicity effect of biosynthesized Fe_2O_3NPs and MgONPs are shown in Table 1 and Fig. 11, 12.

The data presented in the table and figures indicate that all cell lines survived without damage when no solvent (DMSO) was used. However, approximately 5% of cells are damaged after 48 h in the presence of DMSO. We considered HUFP extract as the standard which showed cell damage in less than 95% in both cells. Conversely, green-synthesized Fe_2O_3NPs and MgONPs exhibited significant toxicity towards HeLa cell lines, resulting in only 5% survival after 48 h. Additionally, BHK21 cell lines showed a similar survival rate in MgONPs (5%) but higher survival rates for Fe_2O_3NPs (around 60–70%) after 48 h at the same doses (Fig. 12). This increased toxicity is likely owing to higher nanoparticle doses, as observed in a previous study. The escalating nanoparticle concentration may induce excessive ROS-mediated oxidative stress, leading to DNA damage. This sensitivity to ROS suggests the potential for targeting cancer cells *via* ROS-mediated mechanisms, as cancer cells tend to be more vulnerable than normal cells.[35] Iron and magnesium-based NPs have ROS inducing properties that could selectively eliminate tumor cells and hinder tumor growth. Also, Fe_2O_3NP damages cancer cells (HeLa cell) more than normal cells (BHK-21) whereas MgONP damages both cells equally. This indicates more selectivity of Fe_2O_3NPs than MgONPs towards cancer cells.

Table 1 Qualitative test on HeLa cells and BHK-21 cells

		Cell survival (%)	
Name of sample	Dose (μL)	HeLa cell	BHK-21 cell
Absence of solvent	50	100	100
In presence of solvent	50	>95%	>95%
HUFP extract (standard)	50	>95%	>95%
Fe_2O_3NPs	50 (30 mg mL^{-1})	<5%	60–70%
MgONPs	50 (3 mg mL^{-1})	<5%	<5%

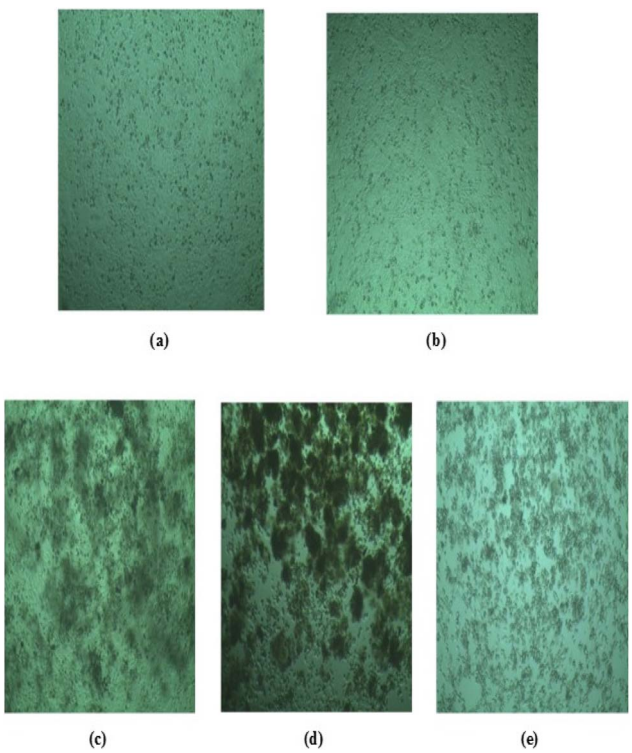

Fig. 11 Anticancer test (qualitative) on HeLa cells: (a) in the absence of solvent, (b) in the presence of solvent, (c) treated with dragon fruit peel extract, (d) treated with Fe_2O_3NPs and (e) treated with MgONPs.

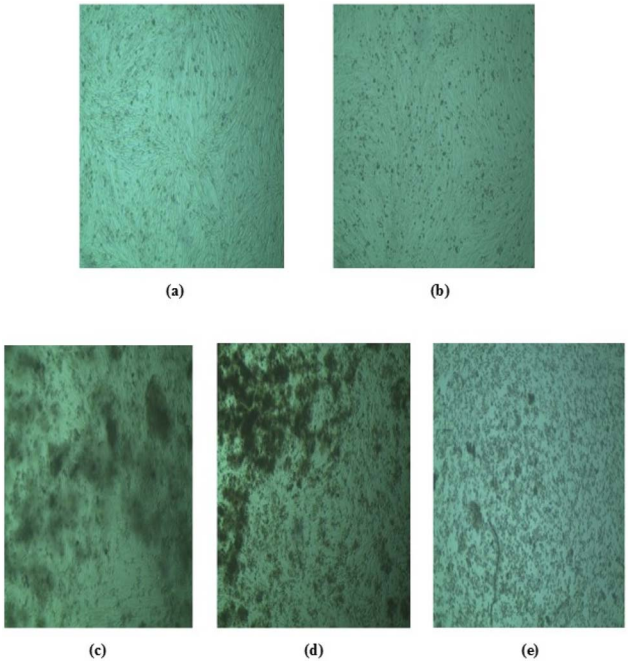

Fig. 12 Anticancer test (qualitative) on BHK-21 cells: (a) in the absence of solvent, (b) in the presence of solvent, (c) treated with dragon fruit peel extract, (d) treated with Fe_2O_3NPs and (e) treated with MgONPs.

Quantitative test (MTT assay) on HeLa cells. Cell viability was assessed after treatment with different concentrations of Fe_2O_3NPs and MgONPs on HeLa cell line using the MTT assay. Fe_2O_3NPs and MgONPs demonstrated a strong cytotoxicity effect for the tested cell line compared with the untreated cell and the cell treated with HUFP extract (standard). Furthermore, higher cell mortality occurs at higher concentrations of the NPs. To check the inhibition effect, the reaction was incubated for 48 h. Fig. 14 and 15 displays the variations in the percentage of inhibition in NPs used to treat HeLa cells. In addition, the cytotoxicity activity effect of Fe_2O_3NPs and MgONPs against HeLa cells were detected by the treatment of different concentrations of the prepared nanoparticles (control, 3.75, 7.5, 15 and 30 mg mL^{-1} for Fe_2O_3NPs and control, 0.375, 0.75, 1.5 and 3 mg mL^{-1} for MgONPs) to check the inhibition of the tumor cells.

The maximum cell growth inhibition (85.97%) was perceived for Fe_2O_3NPs with a concentration of 30 mg mL^{-1} (Fig. 14). On the other hand, maximum cell growth inhibition (85.97%) was perceived for the MgONPs with a concentration of 3 mg mL^{-1} (Fig. 15). The dose-dependent approach (MTT assay) on HeLa cell after treatment with altered concentrations of the prepared Fe_2O_3NPs and MgONPs of HUFP is shown in Fig. 13. The results showed a relationship between the % cell viability and % cell inhibition for HeLa cell lines with the concentration of the NPs. As the concentration of the NPs decreased, the viability of the HeLa cell lines decreased dose-dependently Fig. 13. The detected decrease in cell viability indicates the anticancer properties of Fe_2O_3NPs and MgONPs.[36,37]

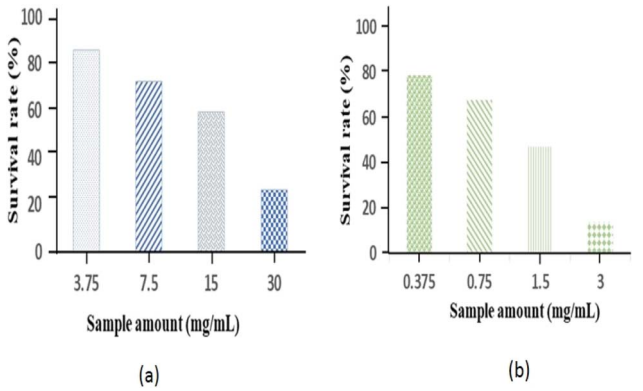

Fig. 13 Quantitative test: survival rate of HeLa cells at different doses of (a) Fe_2O_3NPs and (b) MgONPs.

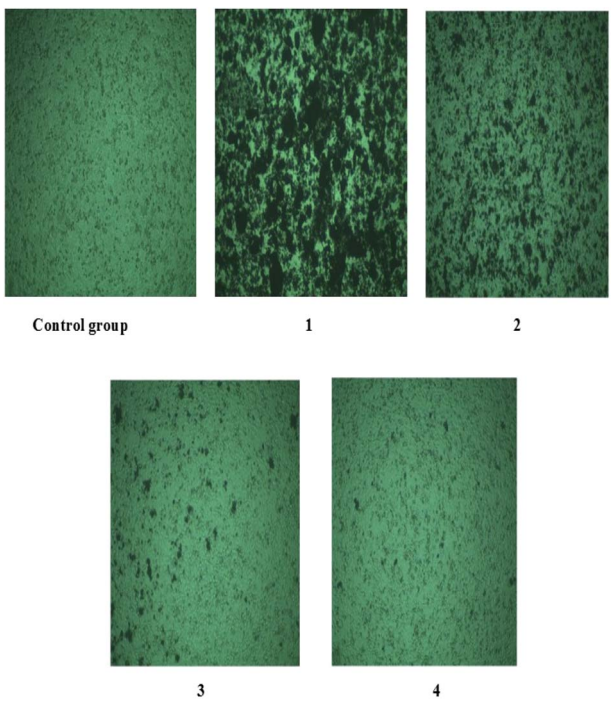

Fig. 14 Quantitative test with Fe_2O_3 NPs: (1) 3.75 mg mL^{-1}, (2) 7.5 mg mL^{-1}, (3) 15 mg mL^{-1}, and (4) 30 mg mL^{-1}.

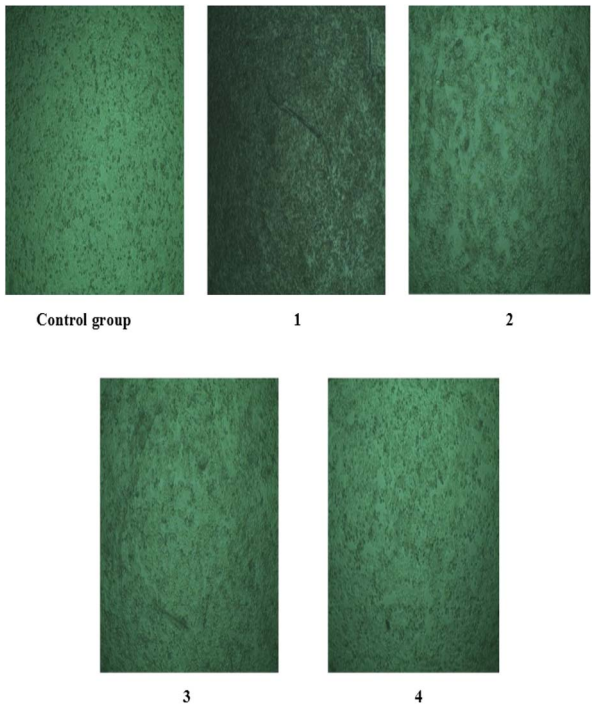

Fig. 15 Quantitative test with MgONPs: (1) 0.375 mg mL^{-1}, (2) 0.75 mg mL^{-1}, (3) 1.5 mg mL^{-1}, and (4) 3 mg mL^{-1}.

Conclusions

This study reports a safe and rapid method for the synthesis and characterization of Fe_2O_3 and MgO nanoparticles using *H. undatus* fruit peel extract. The synthesized nanoparticles showed significant ($p < 0.05$) anticancer activities compared to standard drug and negative control in *in vitro* models. The Fe_2O_3NPs showed more selectivity towards cancer cells than MgONPs but it can be controlled with dose adjustments. The findings of this research indicate that Fe_2O_3 and MgO nanoparticles can be further studied for creating more effective and safe formulations as ideal anticancer drugs.

Data availability

The data that support the findings of this study are available from the corresponding author upon reasonable request.

Author contributions

Sadia Adnin Oyshi: conceived and designed the experiments, performed the experiments, analyzed and interpreted the data and wrote the whole manuscript. Md. Shah Amran and Rumana A. Jahan: analyzed and interpreted the data; contributed reagents, materials, analysis tools or data. Md. Zakir Sultan: reviewed the analysis and interpreted the data. Fahima Aktar and Abu Asad Chowdhury: reviewed the study design and manuscript. Jakir Ahmed Chowdhury and Shaila Kabir: reviewed the analytical data and manuscript.

Conflicts of interest

The authors declare no conflict of interest.

Acknowledgements

The author thanks to Dr Sheikh Ariful Hoque, Principal Scientist of Centre for Advanced Research in Sciences (CARS), University of Dhaka, Bangladesh for his support during anticancer study.

References

1 I. Khan, K. Saeed and I. Khan, Nanoparticles: Properties, applications and toxicities, *Arabian J. Chem.*, 2017, **12**(7), 908–931.
2 K. A. Altammar, A review on nanoparticles: characteristics, synthesis, applications, and challenges, *Front. Microbiol.*, 2023, **14**, 1155622.
3 J. Baranwal, B. Barse, A. Di Petrillo, G. Gatto, L. Pilia and A. Kumar, Nanoparticles in Cancer Diagnosis and Treatment, *Materials*, 2023, **16**(15), 5354.
4 N. Saleh and Z. Yousaf, Tools and techniques for the optimized synthesis, reproducibility and scale up of desired nanoparticles from plant derived material and their role in pharmaceutical properties, *Nanoscale Fabrication, Optimization, Scale-Up and Biological Aspects of Pharmaceutical Nanotechnology*, ed. A. M. Grumezescu, Science-Direct: William Andrew Publishing, 2018, pp. 85–131.
5 C. Pandit, A. Roy, S. Ghotekar, A. Khusro, M. N. Islam, T. B. Emran, *et al.*, Biological agents for synthesis of nanoparticles and their applications, *J. King Saud Univ., Sci.*, 2022, **34**(3), 101869.
6 K. M. Herbach, F. C. Stintzing and R. Carle, Identification of heat-induced degradation products from purified betanin, phyllocactin and hylocerenin by high-performance liquid chromatography/electrospray ionization mass spectrometry, *Rapid Commun. Mass Spectrom.*, 2005, **19**(18), 2603–2616.
7 H. Luo, Y. Cai, Z. Peng, T. Liu and S. Yang, Chemical composition and in vitro evaluation of the cytotoxic and antioxidant activities of supercritical carbon dioxide extracts of pitaya (dragon fruit) peel, *Chem. Cent. J.*, 2014, **8**(1), 1.
8 P. C. Dartsch, A. Kler and E. Kriesl, Antioxidative and antiinflammatory potential of different functional drink concepts in vitro, *Phytother. Res.*, 2008, **23**(2), 165–171.
9 H. Kim, H. K. Choi, J. Y. Moon, Y. S. Kim, A. Mosaddik and S. K. Cho, Comparative antioxidant and antiproliferative activities of red and white pitayas and their correlation with flavonoid and polyphenol content, *J. Food Sci.*, 2011, **76**(1), C38–C45.
10 Y. A. Koksharov, S. P. Gubin, I. V. Taranov, G. B. Khomutov and Y. V. Gulyaev, Magnetic Nanoparticles in Medicine: Progress, Problems, and Advances, *J. Commun. Technol. Electron.*, 2022, **67**(2), 101–116.
11 F. Collin, Chemical Basis of Reactive Oxygen Species Reactivity and Involvement in Neurodegenerative Diseases, *Int. J. Mol. Sci.*, 2019, **20**(10), 2407.
12 R. Fernández-Acosta, C. Iriarte-Mesa, D. Alvarez-Alminaque, B. Hassannia, B. Wiernicki, A. M. Díaz-García, *et al.*, Novel Iron Oxide Nanoparticles Induce Ferroptosis in a Panel of Cancer Cell Lines, *Molecules*, 2022, **27**(13), 3970.
13 B. Kumar, K. Smita, L. Cumbal, A. Debut and Y. Angulo, Biofabrication of copper oxide nanoparticles using Andean blackberry (Rubus glaucus Benth.) fruit and leaf, *J. Saudi Chem. Soc.*, 2017, **21**, S475–S480.
14 A. Pugazhendhi, R. Prabhu, K. Muruganantham, R. Shanmuganathan and S. Natarajan, Anticancer, antimicrobial and photocatalytic activities of green synthesized magnesium oxide nanoparticles (MgONPs) using aqueous extract of Sargassum wightii, *J. Photochem. Photobiol., B*, 2019, **190**, 86–97.
15 V. Daniele, A. R. Volpe, P. Cesare and G. Taglieri, MgO Nanoparticles Obtained from an Innovative and Sustainable Route and Their Applications in Cancer Therapy, *Nanomaterials*, 2023, **13**(22), 2975.
16 M. F. Ananta, S. A. Oyshi, M. M. A. Mim, R. N. Chowdhury, R. Akter, M. A. Rahman, *et al.*, Multipurpose Drug from Rouwolfia serpentina and Nigella sativa: A Herbal Approach to Treat Hypertension and Hyperlipidemia in Experimental Rodent Model, *Journal of Complementary and Alternative Medical Research*, 2023, **24**(4), 9–15.
17 M. S. H. Bhuiyan, M. Y. Miah, S. C. Paul, T. D. Aka, O. Saha, M. M. Rahaman, M. J. I. Sharif, O. Habiba and M. Ashaduzzaman, Green synthesis of iron oxide nanoparticle using Carica papaya leaf extract: application for photocatalytic degradation of remazol yellow RR dye and antibacterial activity, *Heliyon*, 2020, **6**(8), e04603.
18 R. B. Rotti, D. V. Sunitha, R. Manjunath, A. Roy, S. B. Mayegowda, A. P. Gnanaprakash, *et al.*, Green synthesis of MgO nanoparticles and its antibacterial properties, *Front. Chem.*, 2023, **11**, 1–13.
19 L. Permana, P. Sriprom, K. Manamoongmongkol, L. Phumjan and P. Assawasaengrat, Optimization of betalain extraction from dragon fruit (Hylocereus undatus) peel and effect of pH on its properties, *Biomass Convers. Biorefin.*, 2024, **15**, 3545–3556.
20 M. Ramezani Farani, M. Farsadrooh, I. Zare, A. Gholami and O. Akhavan, Green Synthesis of Magnesium Oxide Nanoparticles and Nanocomposites for Photocatalytic Antimicrobial, Antibiofilm and Antifungal Applications, *Catalysts*, 2023, **13**(4), 642.
21 M. Rashid Khan, N. O. Alafaleq, A. K. Ramu, K. Alhosaini, M. S. Khan, T. A. Zughaibi and S. Tabrez, Evaluation of biogenically synthesized MgO NPs anticancer activity against breast cancer cells, *Saudi J. Biol. Sci.*, 2024, **31**(1), 103874.
22 Y. S. Kurniawan, A Fluorescence Study on the Extracts of Red Dragon Fruit Peel in Various Solvents, *Indones. J. Nat. Pigm.*, 2021, **3**(2), 47–51.
23 A. Hussain, M. Yasar, G. Ahmad, M. Ijaz, A. Aziz, M. G. Nawaz, *et al.*, Synthesis, characterization, and

applications of iron oxide nanoparticles, *Int. J. Health Sci.*, 2023, **17**(4), 3–10.

24 B. Boro, A. K. Nath, M. Barthakur and P. Kalita, Synthesis and characterization of MgO nanoparticle and its in vitro cytotoxic effect on erythrocytes, in *Lecture Notes in Bioengineering*, Springer, Singapore, 2020, pp. 199–207.

25 S. O. Aisida, N. Madubuonu, M. H. Alnasir, I. Ahmad, S. Botha, M. Maaza and F. I. Ezema, Biogenic synthesis of iron oxide nanorods using Moringa oleifera leaf extract for antibacterial applications, *Appl. Nanosci.*, 2019, **10**(1), 305–315.

26 H. Liu, P. Li, B. Lu, Y. Wei and Y. Sun, Transformation of ferrihydrite in the presence or absence of trace Fe(II): The effect of preparation procedures of ferrihydrite, *J. Solid State Chem.*, 2009, **182**(7), 1767–1771.

27 S. O. Aisida, N. Madubuonu, M. H. Alnasir, I. Ahmad, S. Botha, M. Maaza and F. I. Ezema, Biogenic synthesis of iron oxide nanorods using Moringa oleifera leaf extract for antibacterial applications, *Appl. Nanosci.*, 2019, **10**(1), 305–315.

28 B. Y. Hirphaye, N. B. Bonka, A. M. Tura and G. M. Fanta, Biosynthesis of magnesium oxide nanoparticles using Hagenia abyssinica female flower aqueous extract for characterization and antibacterial activity, *Appl. Water Sci.*, 2023, **13**, 175.

29 S. Lakshminarayanan, M. F. Shereen, K. L. Niraimathi, P. Brindha and A. Arumugam, One-pot green synthesis of iron oxide nanoparticles from Bauhinia tomentosa: Characterization and application towards synthesis of 1,3 diolein, *Sci. Rep.*, 2021, **11**, 8643.

30 I. Y. Younis, S. S. El-Hawary, O. A. Eldahshan, M. M. Abdel-Aziz and Z. Y. Ali, Green synthesis of magnesium nanoparticles mediated from Rosa floribunda charisma extract and its antioxidant, antiaging and antibiofilm activities, *Sci. Rep.*, 2021, **11**, 16868.

31 S. Yousefi, B. Ghasemi, M. Tajally and A. Asghari, Optical properties of MgO and $Mg(OH)_2$ nanostructures synthesized by a chemical precipitation method using impure brine, *J. Alloys Compd.*, 2017, **711**, 521–529.

32 N. Madubuonu, S. O. Aisida, A. Ali, I. Ahmad, T. Zhao, S. Botha, M. Maaza and F. I. Ezema, Biosynthesis of iron oxide nanoparticles via a composite of Psidium guavaja-Moringa oleifera and their antibacterial and photocatalytic study, *J. Photochem. Photobiol., B*, 2019, **199**, 111601.

33 M. M. Abdel-Aziz, T. M. Emam and E. A. Elsherbiny, Bioactivity of magnesium oxide nanoparticles synthesized from cell filtrate of endobacterium Burkholderia rinojensis against Fusarium oxysporum, *Mater. Sci. Eng., C*, 2020, **109**, 110617.

34 M. Kamaraj, T. Kidane, K. U. Muluken and J. Aravind, Biofabrication of iron oxide nanoparticles as a potential photocatalyst for dye degradation with antimicrobial activity, *Int. J. Environ. Sci. Technol.*, 2019, **16**(12), 8305–8314.

35 S. Mitra, L. N. Nguyen, M. Akter, G. Park, E. H. Choi and N. K. Kaushik, Impact of ROS generated by chemical, physical, and plasma techniques on cancer attenuation, *Cancers*, 2019, **11**(7), 1030.

36 U. S. Gaharwar, R. Meena and P. Rajamani, Biodistribution, clearance and morphological alterations of intravenously administered iron oxide nanoparticles in male Wistar rats, *Int. J. Nanomed.*, 2019, **14**, 9677–9692.

37 M. Amina, N. M. Al Musayeib, N. A. Alarfaj, M. F. El-Tohamy, H. F. Oraby, G. A. Al Hamoud, *et al.*, Biogenic green synthesis of MgO nanoparticles using Saussurea costus biomasses for a comprehensive detection of their antimicrobial, cytotoxicity against MCF-7 breast cancer cells and photocatalysis potentials, *PLoS One*, 2020, **15**(8), e0237567.